Proceedings of 20th International Congress on Acoustics, ICA 2010

23-27 August 2010, Sydney, Australia

Noncontact ultrasonic particle manipulation in a circular trajectory using a vibrating disc

Daisuke Koyama, Yu Ito and Kentaro Nakamura

Precision and Intelligence Laboratory, Tokyo Institute of Technology, 4259-R2-26 Nagatsutacho, Midori-ku, Yokohama, 226-8503 Japan

PACS: 43.25.UV, 43.25.GF, 43.25.QP

ABSTRACT

Noncontact transportation of small particles around a circular trajectory was investigated. A circular aluminum plate with a piezoelectric ring was employed as a vibrating plate. On the basis of finite element analysis (FEA) calculations, the electrodes of the piezoelectric ring were divided into 24 pieces to generate a flexural vibration mode with one nodal circle and four nodal lines at the resonance frequency of 47.8 kHz. A circular plate having the same dimensions as the vibrating plate was installed parallel to the vibrator. It was used as a reflector to generate an acoustic standing wave in the air between the two plates. The acoustic field between the vibrating plate and reflector was calculated by FEA and the distribution of the acoustic radiation force acting on a small rigid particle was calculated to predict the position of the trapped particle. Using a prototype of the vibrating plate, polystyrene particles with diameters of several millimeters could be trapped at regular intervals along the horizontal nodal line of the standing wave. By switching the driving conditions of the divided electrodes in the circumferential direction, the nodal lines of the vibrating plate could be rotated and the trapped particle could be manipulated with a circular trajectory in air.

INTRODUCTION

Ultrasonic noncontact transportation has several advantages over other noncontact transportation techniques based on air pressure and magnetism. One advantage over air-pressure techniques is its superior cost effectiveness because it does not require large amounts of clean air, air compressors, or air tubes. Advantages over magnetic techniques include it does not require generating undesirable external magnetic fields and the transported object does not have to be magnetic.

Several studies have investigated acoustic noncontact particle manipulation techniques [1-4]. Most of them exploit the phenomenon that objects that are small compared with the wavelength of an acoustic standing wave can be trapped at the nodal points of the wave [5-8]. Small particles can be controlled using high-frequency ultrasound [9-14]. However, in this technique, the working distance over which the trapped particle can be controlled is limited to a few wavelengths of the acoustic wave in air due to attenuation of the sound wave. We have been investigating a noncontact technique for transporting small objects over long distances in a linear trajectory [15]. In this technique, small objects can be trapped along the horizontal nodal line of an acoustic standing wave generated between a flexural vibrating plate and a reflector. Controlling the driving phase difference between two transducers attached to either side of the vibrating plate, a flexural traveling wave can be generated and controlled along the plate. In particular, the standing wave in air can be shifted horizontally to transport trapped objects. The motivation behind this present study is the practical application of this noncontact ultrasonic manipulation technique to large-scale manufacturing processes. Such processes often require objects to have nonlinear trajectories. In this paper, noncontact ultrasonic transportation of small objects is discussed. The concept behind this study is depicted in Fig. 1. A proposed noncontact ultrasonic transporter consists of linear transporters reported in a previous study by us [15] and a rotary junction where transported objects can be rotated and their traveling directions can be switched.

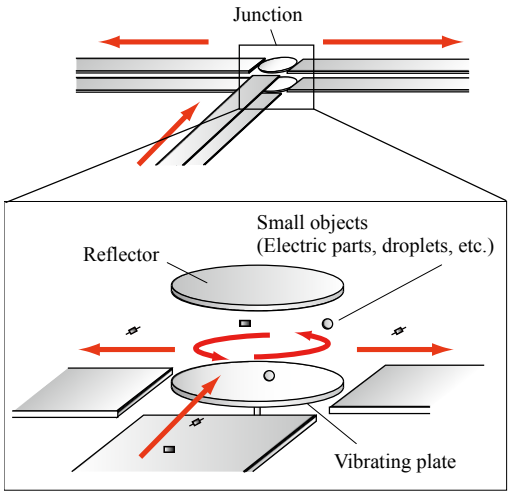

Figure 1. Concept of the noncontact ultrasonic transporter of small objects.

APPARATUS FOR PARTICLE MANIPULATION

The apparatus for manipulating small objects over circular trajectories consists of a circular vibrating plate and a reflector. The configuration of the circular vibrating plate is shown

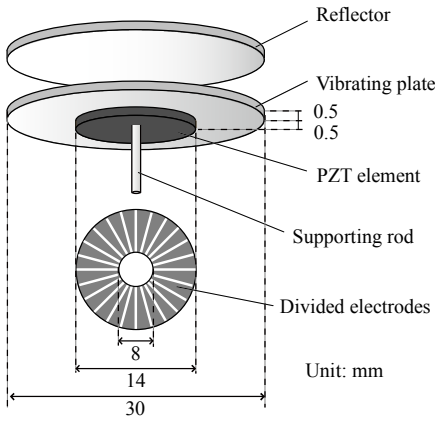

Figure 2. Configuration of a circular vibrating plate.

Table 1. Vibration modes of a circular plate from 18 to 100 kHz predicted by FEA (m: nodal line, n: nodal circle).

$m \diagdown n$	0	1	2	3	4
0			26383	54522	92944
1			37906	69779	
2		20226	50402	97521	
3		34228	64917		
4		47817	86655		
5	18762	60366			
6	26273	73588			
7	35171	88358			
8	45429				
9	57048				
10	70065				
11	84500				

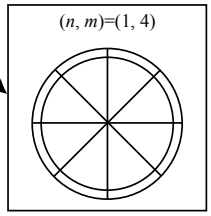

in Fig. 2. A 0.5-mm-thick aluminum disc with a diameter of 30 mm was employed as a vibrating plate and a 0.5-mm-thick piezoelectric zirconate titanate (PZT) ring with inner and outer diameters of 8 and 14 mm respectively, was attached to the vibrating plate by epoxy. To vary the electric driving location of the PZT ring, the surface electrodes of the ring were divided in the circumferential direction. A supporting rod was attached to the center of the circular plate. A 1-mm-thick circular aluminum plate with a diameter of 30 mm was installed parallel to the vibrating plate to generate an acoustic standing wave in the air between the two plates. The vibration mode of the circular plate was investigated by finite element analysis (FEA). The FEA modal analysis results from 18 to 100 kHz are presented in Table 1. Respectively, m and n indicate the number of nodal lines and nodal circles in the resonance vibration modes. The number of nodal lines and circles that appear increase as the resonance frequency increases. In this study, the (n, m) = (1, 4) mode (see illustration in Table 1) at 47.8 kHz was used since it has a larger vibration amplitude than other modes. The number of divided electrodes in the PZT ring was determined to be 24 (see Fig. 2) to correspond to the (1, 4) vibration mode.

FINITE ELEMENT ANALYSIS OF THE ACOUSTIC FIELD

When the (1, 4) flexural vibration mode is excited on the circular plate, an acoustic standing wave will be generated between the vibrating plate and the reflector, allowing a small particle to be trapped at the standing wave nodes. By controlling the driving conditions of the PZT ring, the acoustic field can be varied and the trapped objects will be transported. The circular trajectory of a small object was predicted using FEA to calculate the sound field in the air between the vibrating plate and the reflector. The simulation model of FEA is shown in Fig. 3. The circular vibrating plate and the reflector

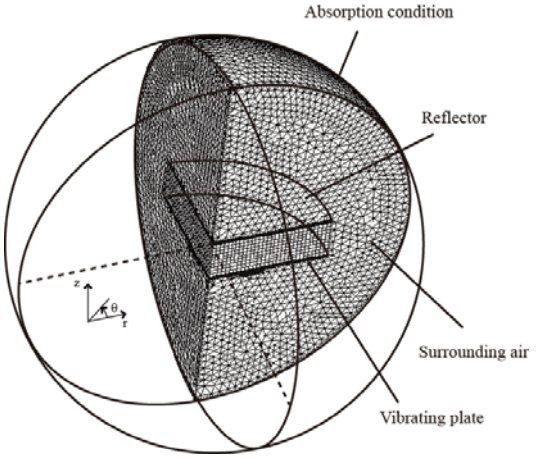

Figure 3. Simulation model of the FEA.

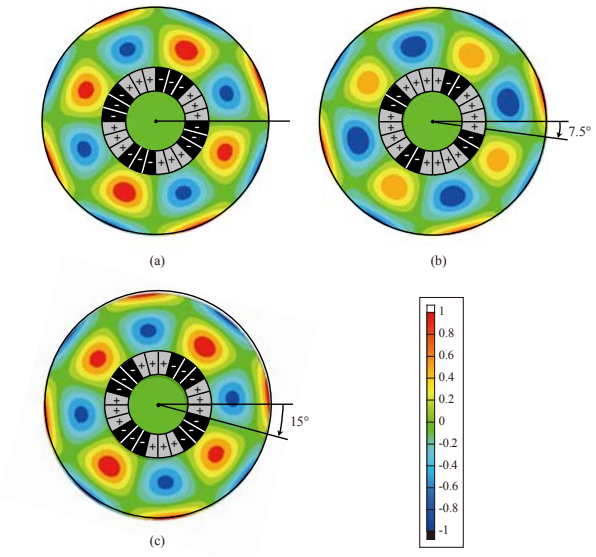

Figure 4. Driving conditions of the PZT electrodes and the calculated vibration amplitude distribution of the circular plate by the FEA at 46.6 kHz.

with diameters of 30 mm were surrounded by an air sphere with diameter of 50 mm. The minimum mesh size was 0.5 mm. The boundary conditions were perfect reflection of sound waves at the reflector surface and absorption without reflection at the surface of the surrounding sphere of air. To reduce the total computational cost, a 1/4 symmetric model was employed by applying symmetric boundary conditions in the r-z plane. The sound pressure distribution in air in the steady state can be calculated using FEA. First, harmonic analysis of the FEA was performed for only the vibrating plate at the resonance frequency of 46.6 kHz. To change the acoustic field between the plate and reflector and control the position of a trapped particle in the circumferential direction the rotation of the vibration distribution on the plate is required. In this present report, the standing wave of the (1, 4) flexural mode was used to control the position of a trapped particle in the circumferential direction by controlling the driving signals. The driving conditions of the PZT ring and the calculated vibration amplitude distribution in the plate are shown in Fig. 4. The symbols "+" and "-" indicate that the divided electrodes were excited with input voltages of V = cosωt and –cosωt, respectively; the aluminum vibrating plate was electrically grounded. The center of the circular plate was fixed and the vibration amplitude was normalized by its maximum value. The FEA results show that the (1, 4) flexural mode, in which a half wavelength corresponds to 45° in the circumferential direction, was generated. As shown in Fig. 4(a), the input voltages of "+" and "-" were alternated every

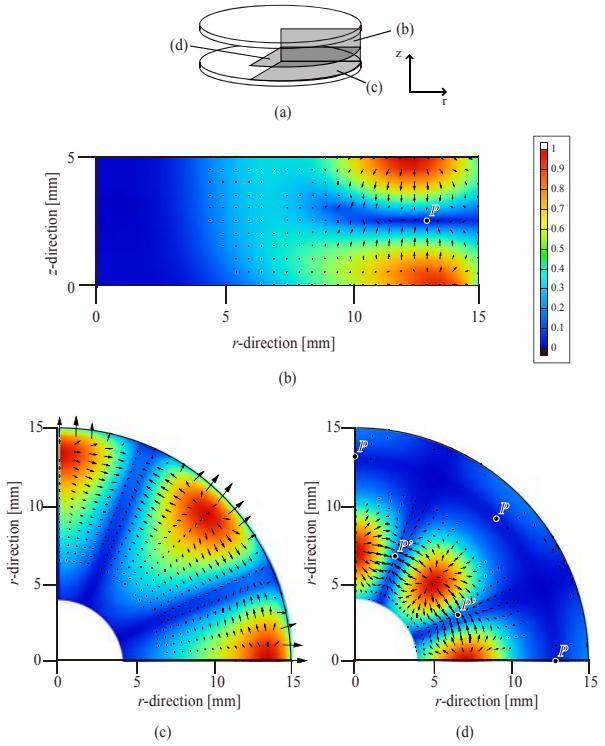

Figure 5. Sound pressure distributions and the vector flows of acoustic radiation force in air between the vibrating plate and the reflector predicted by FEA at 46.6 kHz. (a) Schematic layout of distributions (b)-(d). Distributions in (b) *r-z* plane, (c) *r-θ* plane at $z = 0$ and (d) $z = 2.5$ m

three electrodes (we refer to this driving condition as 3-3 drive). In this case, the angle subtended by three electrode elements (i.e., 45°) corresponds to a half wavelength of the flexural vibration. When one of the input driving signals of the electrodes is changed from "-" to "+" as shown in Fig. 4(b) (called 4-2 drive), the (1, 4) flexural mode is still generated but its nodal lines are rotated 7.5° in the counterclockwise direction. The maximum vibration displacement amplitudes of the plate under these two driving conditions are very similar: the amplitude with 3-3 drive is only 1.8% greater than that with 4-2 drive. Furthermore, when the driving condition was changed from 4-2 drive to 3-3 drive as shown in Fig. 4(c), the (1, 4) mode and nodal lines were rotated by 15° in total. This demonstrates that the acoustic field and the trapped particle can also be rotated in the circumferential direction by controlling the driving condition of the plate. The acoustic radiation force on a small rigid sphere in an acoustic standing wave field F can be expressed as [16]

$$F = VD\nabla\overline{K_E} - V(1-\gamma)\nabla\overline{P_E}\,, \qquad (1)$$

$$D = \frac{3(\rho-\rho_0)}{2\rho+\rho_0}, \qquad (2)$$

where V is the volume of the rigid sphere, ρ is the density of the sphere, ρ_0 is the density of the air, γ is the ratio of the compressibility of air to that of the sphere, $\overline{K_E}$ is the time-averaged kinetic energy, $\overline{P_E}$ is the time-averaged potential energy, and ∇ is the gradient operator. The kinetic energy K_E and the potential energy P_E are expressed as

$$K_E = \frac{1}{2}\rho_0 v^2\,, \qquad (3)$$

$$P_E = \frac{1}{2}\cdot\frac{p^2}{\rho_0 c^2}\,, \qquad (4)$$

where v (= $j/\omega\rho_0$•grad p) is the particle velocity, c is the speed of sound in air, ω is the angular frequency, and p is the sound pressure. It should be noted that the diffraction of sound wave due to the presence of a rigid sphere with a finite size is not taken into consideration in Eqs. (1)–(4). The sound pressure distributions and the vector lines of the acoustic radiation force in air between the vibrating plate and the reflector are shown in Fig. 5. The plate and reflector had a separation of 5 mm to generate an acoustic standing wave between them at 46.6 kHz. The positions of the results in Figs. 5(b)–(d) are indicated in Fig. 5(a). The absolute sound pressure amplitude is shown in each figure. In the *r-θ* plane, an acoustic standing wave was generated in the circumferential direction and the wavelengths and positions of the nodal lines correspond to the vibration distribution of the circular plate. The sound pressure amplitude at a distance of 12 to 13 mm from the center in the r direction was relatively large compared to that at the center of the air layer, and it depends on the vibration distribution of the circular plate shown in Fig. 4. In the *r-z* plane, a standing wave with a half wavelength was also generated. In each figure, the vectors flow out from the loop of the standing wave with the larger sound pressure amplitude. As shown in Fig. 5(b), the vectors flow into the point (r, z) = (13 mm, 2.5 mm) (the point labeled P in Fig. 5(b)) in the *r-z* plane, which is on the horizontal nodal line of the standing wave. Similarly, the results for the *r-θ* plane show that the vector lines flow into the points (r, θ) = (13 mm, 22.5° and 67.5°) in Fig. 5(c) and (13 mm, 0°, 45°, and 90°) (the points labeled P in Fig. 5(d)) and the point (7 mm, 22.5°, and 67.5°) (points labeled P' in Fig. 5(d)). The points that the vectors flow into in Fig. 5(c) are on the surface of the vibrating plate, and the small object will be attracted and contact to the plate at these points. These calculation results predict that the points at which a small object can be trapped are (r, θ, z) = (13 mm, (n-1)×45°, 2.5 mm) and (7 mm, n×22.5°, 2.5 mm) (n = 1, 2…) (i.e., points P and P' in Figs. 5(b) and (d)). There are a total of 16 points around the plate. Point P is more suitable for manipulating particles than point P' because the vertical component of acoustic radiation force is greater at point P than at point P'. The *r-z* plane at n×22.5° corresponds to the nodal plane of the standing wave, and it is difficult to overcome the weight of the manipulated object in order to levitate the object at these points. At point P, the horizontal component of the radiation force in the r direction is approximately 38% of the vertical component in the z direction.

NONCONTACT TRANSPORTATION WITH A CIRCULAR TRAJECTORY

Noncontact transportation of small objects with a circular trajectory was investigated using prototypes of the circular vibrating plate and the reflector. Polystyrene particles with diameters of several millimeters were used as the transported object to observe the spatial relationship between the object and vibrating plate although much smaller particles than the wavelength in air should be employed. The vibration distribution of the plate was measured using a scanning laser Doppler vibrometer (LDV). The (1, 4) flexural vibration mode was generated at 44.5 kHz as shown in Fig. 6(a) and there was good agreement between the experimental results and the FEA results. The maximum vibration displacement amplitude in the vertical direction of the plate driven with an input voltage of 100 V_{pp} was 1.34 μm. The sound pressure amplitude in air between the plate and the reflector was measured by a fiber optic probe. The 125-μm-diameter fiber optic probe could measure the sound pressure without introducing a disturbance. Our results show that the fiber optic probe could

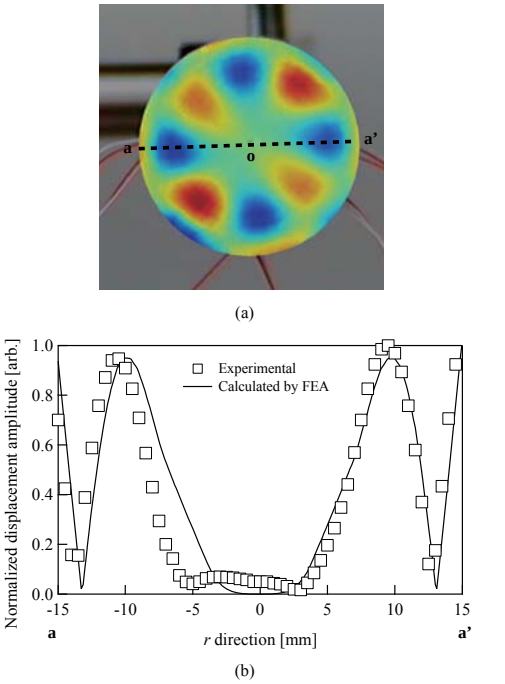

Figure 6. Vibration amplitude distribution of the circular plate at 44.5 kHz.

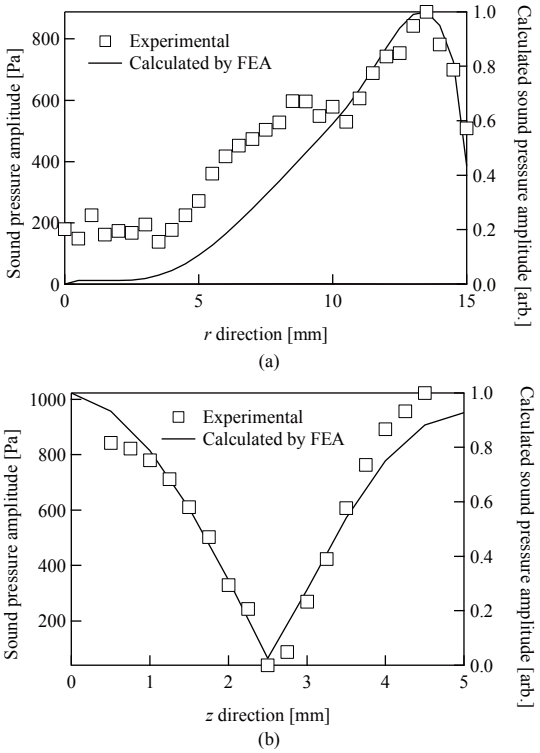

Figure 7. Sound pressure distributions in air between the vibrating plate and the reflector at 44.5 kHz in (a) *r* direction at $z = 0.5$ mm and (b) *z* direction at $r = 13$ mm.

determine the sound pressure by measuring variations in the reflected light intensity from the fiber tip since the reflection coefficient depends on the sound pressure. Details of this probe are given in a previous report by us [17]. The sound pressure amplitude distribution between the plate and the reflector in the *r* direction at $z = 0.5$ mm and in the *z* direction at $r = 13$ mm is shown in Fig. 7. Normalized FEA results are also plotted as solid lines in Fig. 7; the scanning line in the *r* direction corresponds to the o-a' line in Fig. 6(a). The experimental and computed results show good agreement and the maximum sound pressure amplitude in the air layer was approximately 1,000 Pa.

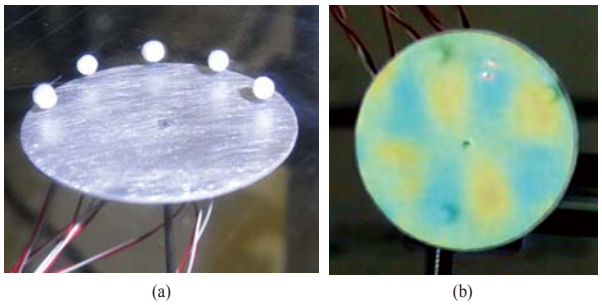

Figure 8. Photographs of polystyrene particles trapped between the vibrating plate and the acrylic transparent reflector. (a) Bird's-eye view, and (b) top-view by the scanning LDV.

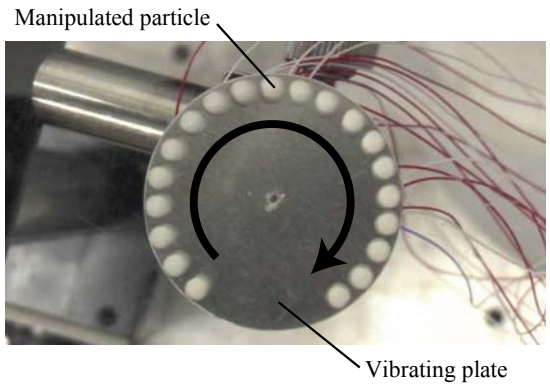

Figure 9. Photograph of a manipulated polystyrene particle at 44.5 kHz.

Noncontact trapping of polystyrene particles was examined by installing a reflector. A photograph of trapped particles between the plate and the reflector is shown in Fig. 8(a). A transparent acrylic plate was employed as the reflector to allow the trapped particles to be easily observed. Fig. 8(b) shows the observational result using the scanning LDV through the reflector from the top view and we can realize the spatial relationship between the trapped positions and the vibration distribution of the plate. The polystyrene particles could be trapped with at regular intervals corresponding to half the wavelength of the flexural vibration of the plate around the circular plate, and it could be confirmed that the points at which the particles were trapped correspond to points *P* predicted by the FEA. The reason why a particle could not be trapped at the equivalent position of *P*' shown in Fig. 5(d) was mentioned in previous section: the vertical component of the acoustic radiation force is less than the weight of the polystyrene particle. Noncontact transportation of the trapped particles was investigated by switching the input signal to the PZT electrodes. The driving conditions of the PZT ring were varied in the same manner as in the FEA (Fig. 4) (i.e., alternating between 3-3 and 4-2 drives). Noncontact transportation of a polystyrene particle with a circular trajectory in the counterclockwise direction could be achieved by switching the driving conditions as shown in Fig. 9. Switching the driving conditions from 3-3 drive to 4-2 drive is counted as a single switch. Photographs taken at every two switches are shown in Fig. 9. The trapped particle was moved by a regular distance in the circumferential direction and the maximum transportation speed was approximately 97 mm/s. The relationship between the number of switches in the input signals and the position of the manipulated particle is presented in Fig. 10. The particle position is expressed as (r, θ) where *r* is the distance from the center of the plate and θ is the center angle from the default position. In the circumferential direction, the moving distance is proportional to the switching time and the manipulated particle is moved through 7.5° each switch, so that 48 switches are

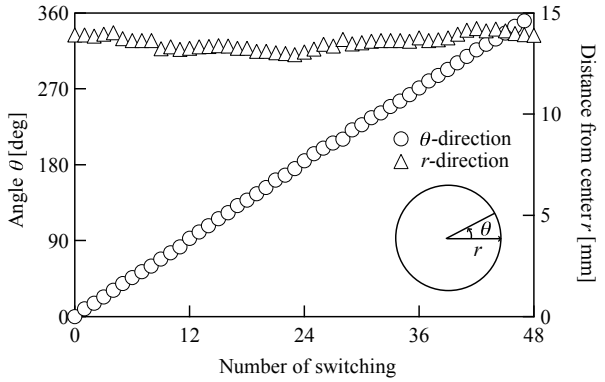

Figure 10. Relationship between the number of switches of the input signal and the position of manipulated particle. The particle position is expressed as (r, θ) (r: distance from the center of the plate, θ: center angle).

required to transport the particle through 360°. This experimental result implies that the acoustic standing wave in air between the vibrating plate and the reflector is rotated by the rotation of (1, 4) flexural vibration of the plate. More precise position control should be possible by increasing the partition number of PZT electrodes. During the circular movement, the position of the manipulated particle in the r direction was approximately r = 13.5 mm, which is close to the calculated result. The traveling particle moved very little in the vertical direction since the acoustic radiation force in the vertical direction far exceeded the weight of the polystyrene particle.

CONCLUSIONS

Noncontact transportation of small particles with a circular trajectory was discussed. The transporter system consists of an aluminum disc with a PZT ring and a reflector. The electrode of the PZT ring was divided into 24 elements to generate and rotate the (1, 4) flexural vibration mode around the plate. The sound pressure distribution and the acoustic radiation force in air between the plate and the reflector were calculated by FEA, and the positions at which a small object can be trapped were predicted. The experiment was carried out with the designed vibrating plate and polystyrene particles with diameters of several millimeters. The particles could be trapped at the positions predicted by the FEA. By switching the input signals to the PZT electrodes, the flexural standing wave could be rotated and a trapped particle could be manipulated around a circular trajectory with an accuracy of 7.5°.

ACKNOWLEDGMENT

This work was partially supported by a research grant from The Murata Science Foundation.

REFERENCES

1 R. R. Whymark, “Acoustic field positioning for containerless processing” *Ultrasonics* **13**, 251-261 (1975)
2 E. G. Lierke, “Acoustic levitation - A comprehensive survey of principles and applications” *Acustica* **82**, 220-237 (1996)
3 H. Hatano, Y. Kanai, Y. Ikegami, T. Fujii and K. Saito, “Fundamental study on ultrasonic levitation and its application to material processing in space” *J. Acoust. Soc. Jpn.* **47**, 40-47 (1991) (in Japanese)
4 E. Benes, M. Gröschl, H. Nowotny, F. Trampler, T. K. Keijizer, H. Böhm, S. Radel, L. Gherardini, J. J. Hawkes, R. König and Ch. Delouvroy, “Ultrasonic separation of suspended particles” *Proc. 2001 IEEE Ultrasonic Symposium* 649-659 (2001).
5 T. Otsuka and T. Nakane, “Ultrasonic levitation for liquid droplet” *Jpn. J. Appl. Phys.***41**, 3259-3260 (2002).
6 A. Haake and J. Dual, “Positioning of small particles by an ultrasound field excited by surface waves” *Ultrasonics* **42**, 75-80 (2004)
7 T. Kozuka, K. Yasui, T. Tuziuti, A. Towata and Y. Iida, “Noncontact acoustic manipulation in air” *Jpn. J. Appl. Phys.* **46**, 4948-4950 (2007)
8 T. Kozuka, K. Yasui, T. Tuziuti, A. Towata and Y. Iida, “Acoustic standing-wave field for manipulation in air” *Jpn. J. Appl. Phys.* **47**, 4336-4338 (2008)
9 M. Takeuchi and K. Yamanouchi, “Ultrasonic micromanipulation of small particles in liquid” *Jpn. J. Appl. Phys.* **33**, 3045-3047 (1994)
10 J. J. Hawkes, J. J. Cefai, D. A. Barrow, W. T. Coakley and L. G. Briarty, “Ultrasonic manipulation of particles in microgravity” *J. Phy. D: App. Phy.* **31**, 1673-1680 (1998)
11 W. T. Coakley, J. J. Hawkes, M. A. Sobanski, C. M. Cousins, and J. Spengler, “Analytical scale ultrasonic standing wave manipulation of cells and microparticles” *Ultrasonics* **38**, 638-641 (2000)
12 A. Haake and J. Dual, “Contactless micromanipulation of small particles by an ultrasound field exited by a vibrating body” *J. Acoust. Soc. Am.* **117**, 2752-2760 (2005)
13 H. Li, J. Friend and L. Yeo, “Surface acoustic wave concentration of particle and bioparticle suspensions” *Biomedical Microdevices* **28**, 4098-4104 (2007)
14 J. Friend, L. Yeo, D. Arifin and Adam Mechler, “Evaporative self-assembly assisted synthesis of polymeric nanoparticles by surface acoustic wave atomization” *Nanotechnology* **19**, 145301 (2008)
15 D. Koyama and K. Nakamura, “Noncontact ultrasonic transportation of small objects over long distances in air using a bending vibrator and a reflector” *IEEE Trans. Ultrason., Ferroelect., Freq. Contr.* **57** 1152-1159 (2010)
16 W. L. Nyborg, “Physical principles of ultrasound” *Ultrasound: Its Applications in Medicine and Biology* (Elsevier Scientific Publishing Company, Amsterdam, 1978), p. 52
17 H. Takei, T. Hasegawa, K. Nakamura and S. Ueha, “Measurement of intense ultraousound field in air using fiber optic probe” *Jpn. J. Appl. Phys.*, **46**, 4555-4557 (2007)